Modal Sound Field Decomposition Applicable for a Limited Range of Directions

Hannes Pomberger, Franz Zotter
Institute of Electronic Music and Acoustics, Email: {pomberger,zotter}@iem.at
University of Music and Performing Arts Graz, Austria

Introduction

The decomposition of spatial sound scenes using spherical microphone arrays is usually based on spherical harmonics. However, the decomposition in spherical harmonics requires a distribution of microphones covering all directions, even if all sources are not all around. For a restricted range of directions the spherical harmonics can be orthogonalized, yielding the spherical Slepian functions. These are well-suited to interpolate data on a partial spherical domain. However, they introduce large errors when extrapolating sound fields with sources outside the restricted range. A different set of orthogonal functions is obtained by solving the Helmholtz equation with an angular boundary condition, e.g. a directional range delimited by an infinite cone that acoustically excludes sources outside. This article discusses the characteristics of the corresponding spherical cap/segment harmonics compared to the spherical harmonics and Slepian functions applied to holographic sound field extrapolation.

Modal sound field decomposition

The Helmholtz equation in spherical coordinates[1] is expressed by $\Delta p(r\boldsymbol{\theta}) - k^2 p(r\boldsymbol{\theta}) = 0$, where Δ is the Laplace operator, $p(r\boldsymbol{\theta})$ is the sound pressure, and k is the wave number. Modal sound field decomposition including all directions is based on the solution of the Helmholtz equation. The angular solutions are usually combined and called spherical harmonics $Y_n^m(\boldsymbol{\theta}) = N_n^{|m|}\, \mathsf{P}_n^{|m|}(\cos\vartheta) \begin{cases} \cos(m\varphi), & \text{for } m \geq 0 \\ \sin(m\varphi), & \text{for } m < 0 \end{cases}$ of order n and degree m; $\mathsf{P}_n^{|m|}$ denotes the associated Legendre functions, and $N_n^{|m|}$ is a scalar normalization term.

A compact spherical microphone array captures the sound pressure distribution on a spherical surface of radius r_M, which can be expressed by a spherical harmonics expansion

$$p(\boldsymbol{r}_M) = \sum_{n=0}^{\infty} \sum_{m=-n}^{n} Y_n^m(\boldsymbol{\theta}) \psi_{nm}. \tag{1}$$

The expansion coefficients are obtained by $\psi_{nm} = \int_{\mathbb{S}^2} Y_n^m(\boldsymbol{\theta})\, p(\boldsymbol{r}_M) d\boldsymbol{\theta}$, where $\mathbb{S}^2$ denotes the unit sphere.

For reproduction, a surrounding spherical loudspeaker array of radius r_L is used to approximate the excitation pattern $f(\boldsymbol{\theta})$ of the captured sound scene, cf. [1]. The spherical harmonics expansion of this excitation pattern is $f(\boldsymbol{\theta}) = \sum_{n=0}^{\infty} \sum_{m=-n}^{n} Y_n^m(\boldsymbol{\theta})\, \phi_{nm}$.

For a microphone array located on a rigid sphere, the coefficients of the excitation pattern and the pressure distribution are connected by, cf. [2], $\psi_{nm} = \frac{-1}{kr_M^2} \frac{h_n(kr_L)}{h_n'(kr_M)}\, \phi_{nm}$. Omitting constant factors, this is accurately approximated at the relevant frequencies as r_L is large by, cf. [3, Eq. 10.52.4],

$$\psi_{nm} = \underbrace{\frac{-i^n e^{-ikr_L}}{k^2 h_n'(kr_M)}}_{w_n(kr_M)}\, \phi_{nm}. \tag{2}$$

Up to a critical frequency, high order modes with $n > \mathrm{N}$ do not contribute significantly in $w_n(kr_M)$. Below this frequency limit the pressure pattern captured by the array is assumed as spatially band-limited, i.e.

$$p(r_M\boldsymbol{\theta}) = \sum_{n=0}^{\mathrm{N}} \sum_{m=-n}^{n} Y_n^m(\boldsymbol{\theta})\, \psi_{nm}. \tag{3}$$

Aliasing is comprehensively discussed in [4]. For simplicity, absence of aliasing is assumed here

For notational convenience, the double sum in the equation above is expressed by a vector product

$$p(r_M\boldsymbol{\theta}) = \boldsymbol{y}_{\mathrm{N}}^{\mathrm{T}}(\boldsymbol{\theta})\boldsymbol{\psi}_{\mathrm{N}}. \tag{4}$$

where $\boldsymbol{y}_{\mathrm{N}}(\boldsymbol{\theta}) := [Y_n^m(\boldsymbol{\theta})]_{q=1\ldots(\mathrm{N}+1)^2}$ and $\boldsymbol{\psi}_{\mathrm{N}} := [\psi_n^m]_{q=1\ldots(\mathrm{N}+1)^2}$ with the linear index $q := n^2 + n + m + 1$. Eq.(2) is expressed by

$$\boldsymbol{\psi}_{\mathrm{N}} = diag\left\{\boldsymbol{w}_{\mathrm{N}}(kr_M)\right\} \boldsymbol{\phi}_{\mathrm{N}}, \tag{5}$$

with $\boldsymbol{w}_{\mathrm{N}}(kr_M) = [w_0(kr_M), \ldots, \overbrace{w_{\mathrm{N}}(kr_M), \ldots, w_{\mathrm{N}}(kr_M)}^{2\mathrm{N}+1}]$ and $\boldsymbol{\phi}_{\mathrm{N}} := [\phi_n^m]_{q=1\ldots(\mathrm{N}+1)^2}$. The pressure pattern expressed in terms of the excitation pattern yields

$$p(r_M\boldsymbol{\theta}) = \boldsymbol{y}_{\mathrm{N}}^{\mathrm{T}}(\boldsymbol{\theta})\, diag\left\{\boldsymbol{w}_{\mathrm{N}}(kr_M)\right\} \boldsymbol{\phi}_{\mathrm{N}}. \tag{6}$$

This work was supported by the project AAP, which was funded by the Austrian ministries BMVIT, BMWFJ, the Styrian Business Agency (SFG), and the departments 3 and 14 of the Styrian Government. The Austrian Research Promotion Agency (FFG) conducts the funding under the Competence Centers for Excellent Technologies (COMET, K-Project), a program of the above mentioned institutions.

[1] Within this article, we define the position vector in terms of spherical coordinates as $\boldsymbol{r} = r\,\boldsymbol{\theta}$, whereby r is the radial distance and $\boldsymbol{\theta}$ is the direction vector $\boldsymbol{\theta} = [\cos(\varphi)\sin(\vartheta), \sin(\varphi)\sin(\vartheta), \cos(\vartheta)]^{\mathrm{T}}$ with φ and ϑ being the azimuth and zenith angle, respectively.

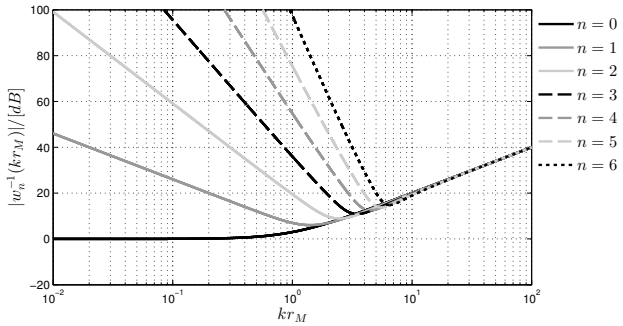

Figure 1: Magnitude response of $w_n^{-1}(kr_M)$ for $n = 0 \dots 6$.

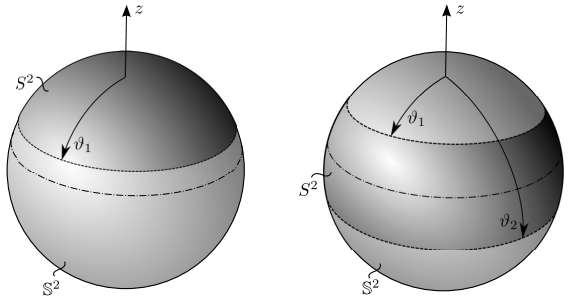

Figure 2: Possible shapes $S^2 \subset \mathbb{S}^2$ for a restriction in ϑ: (a) spherical cap where $\vartheta \leq \vartheta_1$, and (b), and (b) spherical segment where $\vartheta_1 \leq \vartheta \leq \vartheta_2$.

Inverting Eq.(5), the coefficients of the excitation pattern can be calculated from the coefficients of the pressure distribution captured by the array:

$$\boldsymbol{\phi}_{\mathrm{N}} = diag\left\{\boldsymbol{w}_{\mathrm{N}}(kr_M)\right\}^{-1} \boldsymbol{\psi}_{\mathrm{N}}. \tag{7}$$

The magnitude responses of $w_n^{-1}(kr_M)$ for $n = 0 \dots 6$ are depicted in Fig.1.

We are interested in holographic extrapolation for a limited range of directions, especially in a method requiring the same fraction as the surface on which the sound pressure is captured. Let $S^2 \subset \mathbb{S}^2$ denote fractions of the unit sphere delimited only in the zenith angle ϑ. Fig.2 illustrated the two possible shapes, (a) a spherical cap where $\vartheta \leq \vartheta_1$, and (b) a spherical segment where $\vartheta_1 \leq \vartheta \leq \vartheta_2$. The discussion below focuses on two suitable types of orthogonal bases for such fraction and their application to holographic sound field extrapolation.

Spherical Slepian functions

The spherical Slepian functions, cf. [5], form an orthogonal basis for both, the entire sphere and the restricted directional range. The Slepian functions $\boldsymbol{v}_{\mathrm{N}}$ span the same function space as the spherical harmonics and they are related by a transformation matrix $\boldsymbol{U}$

$$\boldsymbol{v}_{\mathrm{N}}(\boldsymbol{\theta}) = \boldsymbol{U}^{\mathrm{T}} \boldsymbol{y}_{\mathrm{N}}(\boldsymbol{\theta}); \tag{8}$$

whereby $\boldsymbol{U}$ contains the eigenvectors of $\boldsymbol{G}$, cf. [5], the Gram-matrix $\boldsymbol{G}$ of the spherical harmonics up to order

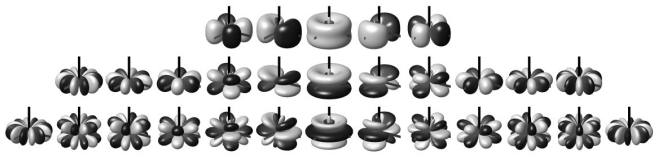

Figure 3: Spherical Slepian functions for a spherical segment with $\vartheta_1 = 60°$, $\vartheta_2 = 120°$, spatially band-limited with $n \leq 6$, and a threshold $\sigma = 0.9$.

$n < \mathrm{N}$ on S^2

$$\boldsymbol{G} = \int\limits_{S^2 \subset \mathbb{S}^2} \boldsymbol{y}_{\mathrm{N}}(\boldsymbol{\theta})\, \boldsymbol{y}_{\mathrm{N}}^{\mathrm{T}}(\boldsymbol{\theta})\, d\boldsymbol{\theta} = \boldsymbol{U}\boldsymbol{\Sigma}\boldsymbol{U}^{\mathrm{T}}. \tag{9}$$

where $\boldsymbol{\Sigma} = diag\left\{[\sigma_i]_{1\dots(\mathrm{N}+1)^2}\right\}$ contains the eigenvalues $\sigma_1 < \ldots < \sigma_{(\mathrm{N}+1)^2}$. On a rotationally symmetric region, the spherical Slepian functions can be determined for each degree m individually.

In contrast to the spherical harmonics, the Slepian functions exhibit an angular energy concentration. Taking a subset of the spherical Slepian functions $\tilde{\boldsymbol{v}}_{\mathrm{N}}(\boldsymbol{\theta}) = [v_i(\boldsymbol{\theta})]_{i=1\dots\mathrm{M}}$, $\mathrm{M} < (\mathrm{N}+1)^2$, yields the subspace of band limited functions exhibiting energy concentration in the region of interest. The energy concentration is adjusted by a threshold σ such that $\frac{\sigma_i}{\max(\sigma_i)} > \sigma$. For this subset Eq.(8) reduces to

$$\tilde{\boldsymbol{v}}_{\mathrm{N}}(\boldsymbol{\theta}) = \tilde{\boldsymbol{U}}^{\mathrm{T}} \boldsymbol{y}_{\mathrm{N}}(\boldsymbol{\theta}). \tag{10}$$

where $\tilde{\boldsymbol{U}}$ is the $(\mathrm{N}+1)^2 \times \mathrm{M}$ part of the transformation matrix, $\boldsymbol{U} = [\tilde{\boldsymbol{U}}, \tilde{\boldsymbol{U}}_{\perp}]$. The spherical Slepian functions for a spherical segment up to order $\mathrm{N} = 6$ are depicted in Fig.3.

Decomposing the captured pressure pattern on S^2 terms of this subset of spherical Slepian functions yields

$$\tilde{\boldsymbol{\psi}}_{\mathrm{N}} = \tilde{\boldsymbol{\Sigma}}^{-1} \int\limits_{S^2 \subset \mathbb{S}^2} \tilde{\boldsymbol{v}}_{\mathrm{N}}(\boldsymbol{\theta})\, p(r_M \boldsymbol{\theta})\, d\boldsymbol{\theta}, \tag{11}$$

whereby $\tilde{\boldsymbol{\Sigma}} = diag\left\{[\sigma_i]_{1\dots\mathrm{M}}\right\}$. The decomposition is numerically stable by choosing σ sufficiently large.

Inserting Eq.(10) in the above equation and expressing the sound pressure pattern in terms of the excitation pattern, cf. Eq.(6), yields

$$\tilde{\boldsymbol{\psi}}_{\mathrm{N}} = \tilde{\boldsymbol{\Sigma}}^{-1}\tilde{\boldsymbol{U}}^{\mathrm{T}} \int\limits_{S^2 \subset \mathbb{S}^2} \boldsymbol{y}_{\mathrm{N}}(\boldsymbol{\theta}) \boldsymbol{y}_{\mathrm{N}}^{\mathrm{T}}(\boldsymbol{\theta}) d\boldsymbol{\theta}\, diag\left\{\boldsymbol{w}_{\mathrm{N}}(kr_M)\right\} \boldsymbol{\phi}_{\mathrm{N}}.$$

Inserting the eigendecomposition of Eq.(9) yields

$$\tilde{\boldsymbol{\psi}}_{\mathrm{N}} = \underbrace{\tilde{\boldsymbol{\Sigma}}^{-1}\tilde{\boldsymbol{U}}^{\mathrm{T}}\, \boldsymbol{U}\, \boldsymbol{\Sigma}\, \boldsymbol{U}^{\mathrm{T}}}_{\tilde{\boldsymbol{U}}^{\mathrm{T}}}\, diag\left\{\boldsymbol{w}_{\mathrm{N}}(kr_M)\right\} \boldsymbol{\phi}_{\mathrm{N}}, \tag{12}$$

whereby the simplification results from the orthogonality of $\boldsymbol{U}$, i.e. $\tilde{\boldsymbol{U}}^{\mathrm{T}}\, \boldsymbol{U} = \left[\boldsymbol{I}_{\mathrm{M}\times\mathrm{M}}\, \boldsymbol{0}_{\mathrm{M}\times(\mathrm{N}+1)^2-\mathrm{M}}\right]$. If we assume that the excitation pattern is suitably angularly limited by the condition $\tilde{\boldsymbol{U}}_{\perp}^{\mathrm{T}} \boldsymbol{\phi}_{\mathrm{N}} = \boldsymbol{0}$, the excitation can be expressed by $\boldsymbol{\phi}_{\mathrm{N}} = \tilde{\boldsymbol{U}}\tilde{\boldsymbol{\phi}}_{\mathrm{N}}$; and the propagation relation for the spherical Slepian functions yields

$$\tilde{\boldsymbol{\psi}}_{\mathrm{N}} = \tilde{\boldsymbol{U}}^{\mathrm{T}}\, diag\left\{\boldsymbol{w}_{\mathrm{N}}(kr_M)\right\} \tilde{\boldsymbol{U}}\tilde{\boldsymbol{\phi}}_{\mathrm{N}}. \tag{13}$$

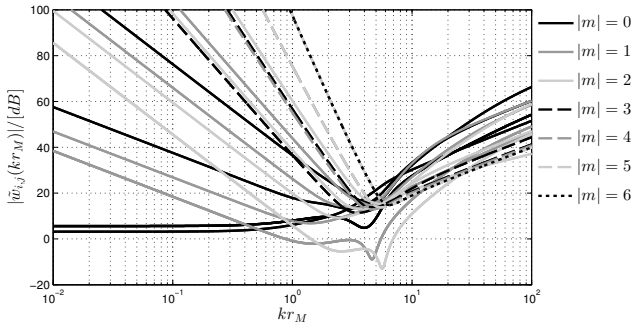

Figure 4: Magnitude response of $\tilde{w}_{i,j}(kr_M)$ for $n \leq 6$; the corresponding basis functions are depicted in Fig.3

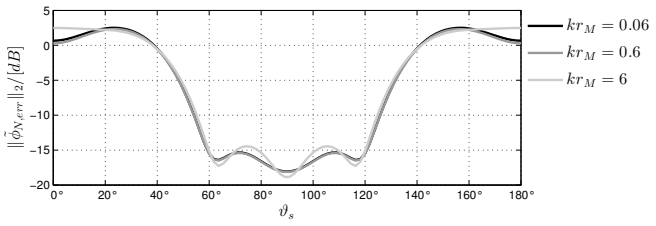

Figure 5: Energy of the error in the excitation pattern $\tilde{\boldsymbol{\phi}}_{\mathrm{N,err}}$, cf. Eq.(15) , for a plane wave impinging from ϑ_s for an array located on a spherical segment with $\vartheta_1 = 60°$, $\vartheta_2 = 120°$

The inverse yields the coefficients of the excitation pattern $\tilde{\boldsymbol{\phi}}_{\mathrm{N}}$ from the coefficients of the pressure $\tilde{\boldsymbol{\psi}}$:

$$\tilde{\boldsymbol{\phi}}_{\mathrm{N}} = \underbrace{\left[\tilde{\boldsymbol{U}}^{\mathrm{T}}\, diag\left\{\boldsymbol{w}_{\mathrm{N}}(kr_M)\right\}\tilde{\boldsymbol{U}}\right]^{-1}}_{:=\tilde{W}=[\tilde{w}_{i,j}(kr_M)]_{M\times M}} \tilde{\boldsymbol{\psi}}_{\mathrm{N}}. \qquad (14)$$

In contrast to capture on the full sphere, cf. Eq.(7), partial capture and holography requires a frequency dependent matrix inversion when using spherical Slepian functions.

Fig.4 depicts the magnitude response of $\tilde{w}_{i,j}(kr_M)$, cf. Eq.(14) for Slepian functions on a spherical segment, $n \leq$ N, cf. Fig.3.

An error occurs if the excitation pattern is not fulfilling the condition $\tilde{\boldsymbol{U}}_{\perp}^{\mathrm{T}}\boldsymbol{\phi}_{\mathrm{N}} \neq \boldsymbol{0}$. Such patterns cause sound pressure patterns captured on S^2, which are misinterpreted. By subtracting[2] Eq.(12) from Eq.(13), $\tilde{\boldsymbol{\psi}}_{\mathrm{N,err}} = \tilde{\boldsymbol{U}}^{\mathrm{T}}\, diag\left\{\boldsymbol{w}_{\mathrm{N}}(kr_M)\right\}\tilde{\boldsymbol{U}}_{\perp}\tilde{\boldsymbol{U}}_{\perp}^{\mathrm{T}}\boldsymbol{\phi}_{\mathrm{N}}$ and inserting into Eq.(14) defines the erroneous contribution to $\tilde{\boldsymbol{\phi}}_{\mathrm{N}}$

$$\tilde{\boldsymbol{\phi}}_{\mathrm{N,err}} = \tilde{\boldsymbol{W}}\,\tilde{\boldsymbol{U}}^{\mathrm{T}}\, diag\left\{\boldsymbol{w}_{\mathrm{N}}(kr_M)\right\}\tilde{\boldsymbol{U}}_{\perp}\tilde{\boldsymbol{U}}_{\perp}^{\mathrm{T}}\boldsymbol{\phi}_{\mathrm{N}}. \qquad (15)$$

Fig.5 shows the energy of $\tilde{\boldsymbol{\phi}}_{\mathrm{N,err}}$ for a plane wave in dependence of its zenith angle of incidence ϑ_s on an array located on a spherical segment with $\vartheta_1 = 60°$, $\vartheta_2 = 120°$.

Spherical cap/segment harmonics

Imposing sound-hard boundary conditions in ϑ on the Helmholtz equation restricts the limited range of directions $S^2 \subset \mathbb{S}^2$ to a spherical cap, cf. [6], or segment and yields an orthogonal and complete basis on S^2.

[2]Note that $\boldsymbol{I} - \tilde{\boldsymbol{U}}\tilde{\boldsymbol{U}}^{\mathrm{T}} = \tilde{\boldsymbol{U}}_{\perp}\tilde{\boldsymbol{U}}_{\perp}^{\mathrm{T}}$.

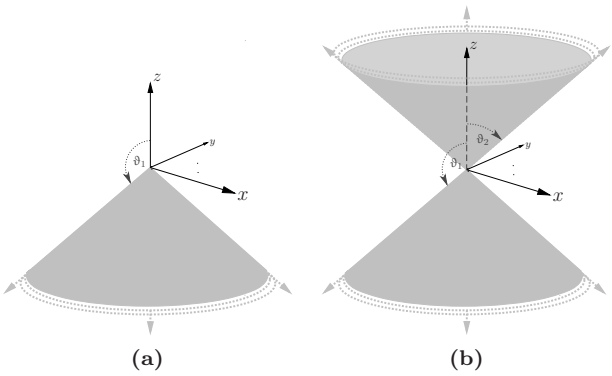

Figure 6: (a) semi-infinite cone and (b) infinite double cone.

The angular solutions of the Helmholtz equation fulfilling such a boundary condition are the spherical cap/segment harmonics

$$Y^m_{\nu_l(m)}(\boldsymbol{\theta}) = N^{|m|}_{\nu_l(m)}\, P^{|m|}_{\nu_l(m)}(\cos\vartheta) \begin{cases} \sin(m\varphi), & \text{for } m < 0, \\ \cos(m\varphi), & \text{for } m > 0, \end{cases} \qquad (16)$$

where $P^{|m|}_{\nu_l(m)} = \mathsf{P}^{|m|}_{\nu_l(m)} + \alpha_l(m)\,\mathsf{Q}^{|m|}_{\nu_l(m)}$; P^m_ν, Q^m_ν are the associated Legendre functions of non-integer order ν and α is a scalar weight depending on the type of boundary condition. An algorithm for computing the associated Legendre functions of non-integer order is given in [7].

Semi-infinite cone. A semi-infinite conical scatterer, cf. Fig.6(a), corresponds to the boundary condition $\left.\frac{\partial p(r\boldsymbol{\theta})}{\partial\vartheta}\right|_{\vartheta=\vartheta_1} = 0$. As this condition concerns only ϑ it reduces to

$$\left.\frac{\partial\, P^{|m|}_{\nu_l(m)}(\cos\vartheta)}{\partial\vartheta}\right|_{\vartheta=\vartheta_1} = 0. \qquad (17)$$

There is an infinite but discrete set of parameters $\nu_l(m)$ and $\alpha_l(m)$, $l = 1\ldots\infty$, for which the boundary condition is fulfilled. Restricting the functions to be finite in S^2, requires $\alpha_l(m)$ to be zero as $|\,\mathsf{Q}^m_\nu(\cos\vartheta)| \to \infty$ for $\vartheta \to 0$.

The zeros of $f(\nu) = \frac{\partial\,\mathsf{P}^{|m|}_\nu(\cos\vartheta_1)}{\partial\vartheta}$ determine the values of $\nu_l(m)$. For this purpose a numerical zero-finding algorithm is used, e.g. MATLAB's *fzero* (derivatives of Legendre functions can be evaluated using one of their recurrence relations, cf. [3, Eq. 14.10.5]).

Infinite double cone. Similarly, an infinite double conical scatterer, cf. Fig.6(b), corresponds to the boundary conditions $\left.\frac{\partial\, P^{|m|}_{\nu_l(m)}(\cos\vartheta)}{\partial\vartheta}\right|_{\vartheta=\vartheta_{1,2}} = 0$, which is equivalent to

$$\left[\frac{\partial\,\mathsf{P}^{|m|}_{\nu_l(m)}(\cos\vartheta)}{\partial\vartheta} + \alpha_l(m)\frac{\partial\,\mathsf{Q}^{|m|}_{\nu_l(m)}(\cos\vartheta)}{\partial\vartheta}\right]_{\vartheta=\vartheta_{1,2}} = 0. \qquad (18)$$

By evaluating at both boundaries α can be eliminated. The zeros of the remaining expression $f(\nu) =$

Figure 7: Spherical segment harmonics for a double conical boundary condition $\theta_1 = 60°$, $\theta_2 = 120°$, and spatially band-limited with $\nu_q \leq 6$.

$\frac{\partial \mathsf{P}_\nu^{|m|}(\cos\vartheta_1)}{\partial\vartheta}\frac{\partial \mathsf{Q}_\nu^{|m|}(\cos\vartheta_2)}{\partial\vartheta} - \frac{\partial \mathsf{P}_\nu^{|m|}(\cos\vartheta_2)}{\partial\vartheta}\frac{\partial \mathsf{Q}_\nu^{|m|}(\cos\vartheta_1)}{\partial\vartheta}$ determine the values of $\nu_l(m)$. Based on $\nu_l(m)$ the values of $\alpha_l(m)$ are determined by Eq.(18).

The spherical segment harmonics for a double cone with $\vartheta_1 = 60°$, $\vartheta_2 = 120°$, up to order $\mathrm{N} = 6$ are depicted in Fig.7.

Modal sound field decomposition. On spherical cap/segment $S^2 \subset \mathbb{S}^2$ restricted by the boundary, the spherical cap/segment harmonics are orthonormal, $\int_{S^2\subset\mathbb{S}^2} Y^{m'}_{\nu_l'(m')}(\boldsymbol{\theta}) Y^{m}_{\nu_l(m)}(\boldsymbol{\theta})\, d\boldsymbol{\theta} = \delta_{ll'}\delta_{mm'}$, and complete, $\int_{S^2\subset\mathbb{S}^2}[f(\boldsymbol{\theta}) - \sum_{l=0}^{\infty}\sum_{m=-l}^{l} Y^{m}_{\nu_l(m)}(\boldsymbol{\theta})\,\hat{\phi}_{lm}]^2 d\boldsymbol{\theta} = 0$, where $\hat{\phi}_{lm} = \int_{S^2\subset\mathbb{S}^2} f(\boldsymbol{\theta}) Y^{m}_{\nu_l(m)}(\boldsymbol{\theta})\, d\boldsymbol{\theta}$ are the expansion coefficients.

For notational convenience, we introduce the linear index $q \in 1\ldots\mathrm{Q}$ and $\nu_q = \nu_l(m)$ with $\nu_1 < \nu_2 < \ldots < \nu_\mathrm{Q} \leq \mathrm{N}$ and m_q, ψ_q are the associated degrees and expansion coefficients . This allows to express the spatially band limited pressure pattern by

$$p(r_M\boldsymbol{\theta}) = \hat{\boldsymbol{y}}_\mathrm{N}^\mathrm{T}(\boldsymbol{\theta})\hat{\boldsymbol{\psi}}_\mathrm{N}, \tag{19}$$

where $\hat{\boldsymbol{y}}_\mathrm{N}(\boldsymbol{\theta}) := [Y^0_{\nu_1}(\boldsymbol{\theta}), \ldots, Y^{m_\mathrm{Q}}_{\nu_\mathrm{Q}}(\boldsymbol{\theta})]$, and $\hat{\boldsymbol{\psi}}_\mathrm{N} := [\hat{\psi}_1, \ldots, \hat{\psi}_\mathrm{Q}]$. The spherical cap/segment harmonics expansion of the corresponding excitation pattern yields

$$f(\boldsymbol{\theta}) = \hat{\boldsymbol{y}}_\mathrm{N}^\mathrm{T}(\boldsymbol{\theta})\hat{\boldsymbol{\phi}}_\mathrm{N}, \tag{20}$$

where $\hat{\boldsymbol{\phi}}_\mathrm{N} := [\hat{\phi}_1, \ldots, \hat{\phi}_\mathrm{Q}]$.

An array capturing the spherical cap/segment spectrum of the sound pressure at the radius r_M receives

$$\hat{\boldsymbol{\psi}}_\mathrm{N} = diag\left\{\hat{\boldsymbol{w}}_\mathrm{N}(kr_M)\right\}\hat{\boldsymbol{\phi}}_\mathrm{N}, \tag{21}$$

with $\hat{\boldsymbol{w}}_\mathrm{N}(kr_M) = [\hat{w}_0(kr_M), \ldots, \hat{w}_\mathrm{Q}(kr_M)]$ and

$$\hat{w}_q(kr_M) = \frac{-i^{\nu_q} e^{-ikr_L}}{k^2 h'_{\nu_q}(kr_M)}. \tag{22}$$

The radial propagation terms in the above equation are similar to the spherical case, Eq.(5), with the only difference of a non-integer parameter ν_q. As the propagation terms behave similarly, the spatial band-limitation is motivated by the same reason as for the spherical case.

The coefficients of the excitation pattern can be calculated from $\hat{\boldsymbol{\psi}}_\mathrm{N}$ by inverting Eq.(21),

$$\hat{\boldsymbol{\phi}}_\mathrm{N} = diag\left\{\hat{\boldsymbol{w}}_\mathrm{N}(kr_M)\right\}^{-1}\hat{\boldsymbol{\psi}}_\mathrm{N}. \tag{23}$$

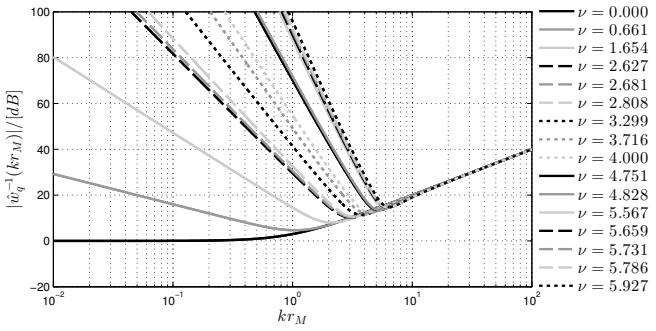

Figure 8: Magnitude response of $w_q^{-1}(kr_M)$ for $\nu_q \leq 6$; the corresponding basis functions are depicted in Fig.7

Comparing the above equation with Eq.(7), reveals that the expressions are structurally identical. However band limitation has different consequences in the spherical cap/segment harmonics than in he spherical harmonics. Fig.8 depicts the magnitude responses of $w_q^{-1}(k)$ for a double conical boundary and $\nu_q \leq 6$.

Conclusion and prospects

Modal sound field decomposition and holographic extrapolation are applicable to both, spherical Slepian functions and spherical cap/segment harmonics. However, extrapolating spherical Slepian functions requires a frequency dependent matrix inversion and provokes large errors when sources are located outside the directional range of interest. In contrast, extrapolating spherical cap/segment harmonics is structurally identical to spherical harmonics. Theoretically, the physical boundary excludes sources outside. Extrapolating spherical cap/segment harmonics using conical boundaries of finite extent will be investigated in future work.

References

[1] F. Zotter, H. Pomberger, and M. Frank, "An alternative ambisonics formulation: Modal source strength matching and the effect of spatial aliasing," in *Proc of 126nd AES Conv.*, 2009.

[2] R. Baumgartner, H. Pomberger, and M. Frank, "Practical implementation of radial filters for ambisonic recordings," in *Proc. of ICSA, Detmold*, 2011.

[3] "NIST Digital Library of Mathematical Functions," http://dlmf.nist.gov/, Release 1.0.5 of 2012-10-01. [Online]. Available: http://dlmf.nist.gov/

[4] B. Rafaely, B. Weiss, and E. Bachmat, "Spatial aliasing in spherical microphone arrays," *IEEE Trans. on Signal Proc.*, vol. 55, no. 3, 2007.

[5] F. Zotter and H. Pomberger, "Spherical slepian functions for approximation of spherical measurement data," in *Fortschritte der Akustik*, 2012.

[6] C. Hwang and S. Chen, "Fully normalized spherical cap harmonics: Application to the analysis of sea-level data from TOPEX/POSEIDON and ERS-1," *Geophys. J. Int.*, vol. 129, no. 2, 1997.

[7] F. Olver and J. Smith, "Associated legendre functions on the cut," *J. of comput. phys.*, vol. 51, no. 3, 1983.